Available online at www.sciencedirect.com
SCIENCE DIRECT®
Earth and Planetary Science Letters 241 (2006) 617–633
EPSL
www.elsevier.com/locate/epsl

Low-degree melting of a metasomatized lithospheric mantle for the origin of Cenozoic Yulong monzogranite-porphyry, east Tibet: Geochemical and Sr–Nd–Pb–Hf isotopic constraints

Yao-Hui Jiang *, Shao-Yong Jiang, Hong-Fei Ling, Bao-Zhang Dai

State Key Laboratory for Mineral Deposits Research, Department of Earth Sciences, Nanjing University, Nanjing 210093, China

Received 24 June 2005; received in revised form 14 November 2005; accepted 14 November 2005
Available online 20 December 2005
Editor: S. King

Abstract

SHRIMP zircon U–Pb dating, mineral chemical, element geochemical and Sr–Nd–Pb–Hf isotopic data have been determined for the Yulong monzogranite-porphyry in the eastern Tibet, China. The Yulong porphyry was emplaced into Triassic strata at about 39 Ma. The rocks are weakly peraluminous and show shoshonitic affinity, i.e., alkalis-rich, high K_2O contents with high K_2O/Na_2O ratios, enrichment in LREE and LILE. They also show some affinities with the adakite, e.g., high SiO_2 and Al_2O_3, and low MgO contents, depleted in Y and Yb, and enrichment in Sr with high Sr/Y and La/Yb ratios, and no Eu anomalies. The Yulong porphyry has radiogenic $^{87}Sr/^{86}Sr$ (0.7063–0.7070) and unradiogenic $^{143}Nd/^{144}Nd$ ($\varepsilon_{Nd} = -2.0$ to -3.0) ratios. The Pb isotopic compositions of feldspar phenocrysts separated from the Yulong porphyry show a narrow range of $^{206}Pb/^{204}Pb$ ratios (18.71–18.82) and unusually radiogenic $^{207}Pb/^{204}Pb$ (15.65–15.67) and $^{208}Pb/^{204}Pb$ (38.87–39.00) ratios. In situ Hf isotopic composition of zircons that have been SHRIMP U–Pb dated is characterized by clearly positive initial ε_{Hf} values, ranging from +3.1 to +5.9, most between +4 and +5. Phenocryst clinopyroxene geothermometry of the Yulong porphyry indicates that the primary magmas had anomalously high temperature (>1200 °C). The source depth for the Yulong porphyry is at least 100 km inferred by the metasomatic volatile phase (phlogopite–carbonate) relations. Detailed geochemical and Sr–Nd–Pb–Hf isotopic compositions not only rule out fractional crystallization or assimilation-fractional crystallization processes, but also deny the possibility of partial melting of subducted oceanic crust or basaltic lower crust. Instead, low degree (1–5%) partial melting of a metasomatized lithosphere (phlogopite–garnet clinopyroxenite) is compatible with the data. This example gives a case study that granite can be derived directly by partial melting of an enriched lithospheric mantle, which is important to understand the source and origin of diverse granites.

Keywords: granite; geochemistry; Sr–Nd–Pb–Hf isotopes; metasomatized lithospheric mantle; East Tibet

1. Introduction

Granites play a major role in the evolution of the continental crust and in the beneficial concentration of economic quantities of important materials. However, granitic rocks display great diversity, the source of which, even today, is still one of the most debated subjects in granite petrogenesis. The consensus view

* Corresponding author. Tel.: +86 25 83686584; fax: +86 25 83592393.
E-mail addresses: yhj186@hotmail.com (Y.-H. Jiang), shyjiang@public1.ptt.js.cn (S.-Y. Jiang).

0012-821X/$ - see front matter © 2005 Elsevier B.V. All rights reserved.
doi:10.1016/j.epsl.2005.11.023

is that granites are typically generated during periods of heat and/or mass transfer from the mantle to the crust, either by partial melting of crustal rocks or by fractional crystallization (FC) or assimilation combined with fractional crystallization (AFC) of mantle-derived basaltic magmas (e.g. [1–5]). Nevertheless, the evidence for direct contribution of mantle-derived magmas in granite production is often circumstantial. The studies over the past last decade have also shown that granitic rocks could be generated by partial melting of young subducted oceanic crust during subduction (e.g. [6]). The Archaean tonalite–trondhjemite–granodiorite magmas are also proposed to be directly linked to slab-melting (e.g. [7]), although there exists some controversy on this topic (e.g. [8]). It is, however, considerably uncertain or argumentative whether the granites could have been generated directly by partial melting of the lithospheric mantle.

The Tibetan plateau is the product of the continuing collision of India with the southern margin of Eurasia during the past 65 my. The Cenozoic magmatism is extensive and granitic intrusions and potassic volcanic rocks are widely distributed in the Tibetan plateau (e.g. [9,10]). At least 3 petrogenesis mechanisms for the origin of granite in the Tibet plateau have been proposed: (1) crustal anatexis during continental collision (e.g. [11]); (2) high-temperature crustal anatexis related to asthenospheric upwelling and mantle attenuation [12]; (3) partial melting of a thickened lower crustal rocks triggered by underplating of ultra-potassic magma during slab-breakoff [10].

The Cenozoic Yulong monzogranite-porphyry (YP) is distributed in eastern Tibetan plateau, which hosts the largest porphyry copper deposit in China. This deposit was discovered in late 1960s, and since then it has been subjected to intensive exploration and studies, although the porphyry petrogenesis remains controversial. Ma [13] and Tang and Luo [14] suggested that the YP is calc-alkaline and may have been derived by AFC of mantle-derived basaltic magma. However, Hou et al. [15] argued that the YP is adakitic rocks and must have been originated from direct melting of subducted oceanic crust. In order to better constrain the petrogenesis of the YP and thus to understand better the ore genesis of this largest porphyry copper deposit of China, we investigated a detailed SHRIMP zircon U–Pb dating, mineral chemistry, and major, trace elemental, and Sr–Nd–Pb–Hf isotopic geochemistry for the porphyry. These data strongly suggest that this monzogranite-porphyry shows shoshonitic affinity and was derived directly by partial melting of a metasomatized lithospheric mantle.

2. Geological setting and geology of the YP

2.1. Geological setting

The Tibetan plateau is the largest uplifted structure on Earth. It is bounded to the north by the Altyn Tagh fault and the Tarim block and to the south by the Himalayas [10]. Forming in response to the India–Asia collision, it consists of a series of east–west trending crustal terranes that were successively accreted to the southern margin of Eurasia since the Early Palaeozoic, from north to south, these are the Songpan-Ganze, Qiangtang, and Lhasa terranes (Fig. 1a; [10]). The YP is located in the Qiangtang terrane of the eastern Tibetan plateau (Fig. 1a). The Qiangtang terrane is bound by the Jinshajiang Suture that was formed in the Permian and the Bangong-Nujiang Suture that was formed in Middle Jurassic time [16]. In eastern Tibet, the Qiangtang terrane consists of a Proterozoic crystalline basement and an Early Paleozoic folded basement. The Devonian to Permian platform transitional facies carbonate and clastic sedimentary rocks comprise their cover rocks. On the eastern side of the Qiangtang terrane, there exists a magmatic arc composed of Permian volcano-sedimentary sequence related to the Jinshajiang suture, which is unconformably covered by a Late Triassic flyschoid complex and is locally overthrust onto folded crystalline basement [16].

The Paleocene India-Asia continental collision formed the Indus-Yarlung-Zangbo Suture and resulted in the Jinshajiang strike-slip fault system, which is composed of a number of branches including the Chesuo, Wenquan, and Tuoba faults (Fig. 1b). A series of Cenozoic (49–30 Ma) porphyry bodies occur in this part of orogen (Fig. 1b), which comprise a part of the Ailaoshan-Jinshajiang Cenozoic alkali-rich porphyry belt (Fig. 1a). These porphyry bodies are all enriched in alkaline elements. They were typically emplaced into Triassic volcanic and sedimentary sequences with relatively shallow emplacement depths. This porphyry belt is distributed along with the strike-slip faults and bordered by some strike-slip pull-apart basins with the Gonjo basin on the eastern side, and the Nangqen and Lawu basins on the western side (Fig. 1b). Within the basins there exists a more than 4000-m-thick, Tertiary gypsum-bearing red molasse formation intercalated with alkaline volcanic rocks that show K–Ar ages of 42.4–37.5 Ma (Fig. 1b). Some porphyry bodies within the Ailaoshan-Jinshajiang Cenozoic alkali-rich porphyry belt to the southeast of Yulong contain a series of upper mantle xenoliths such as phlogopite–garnet clinopyroxenite

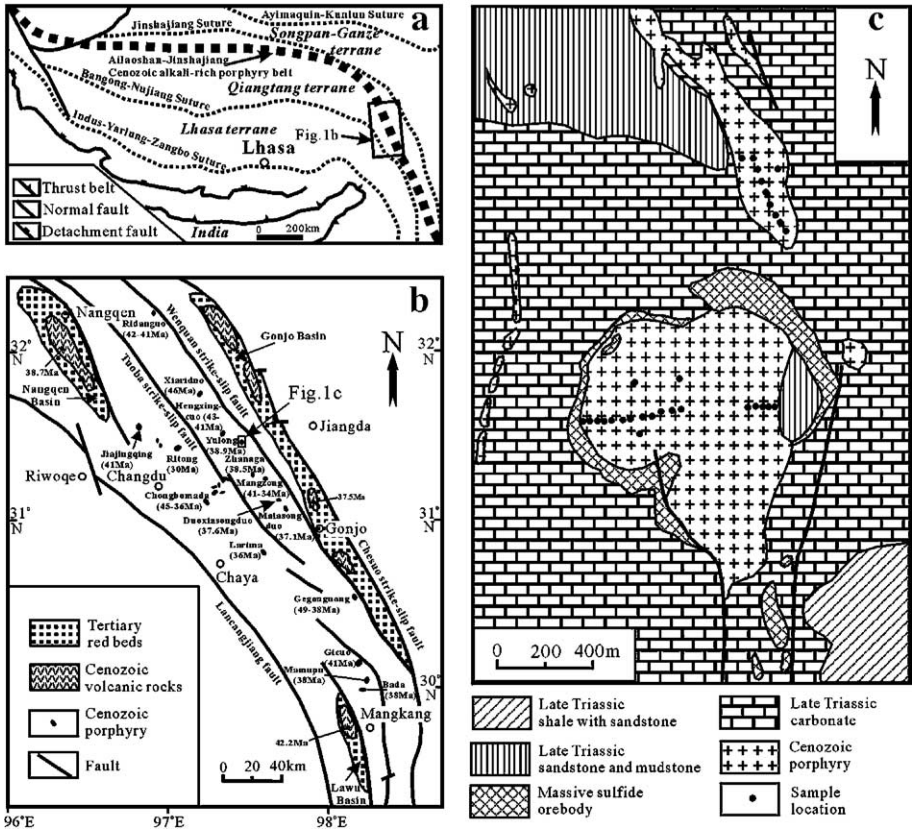

Fig. 1. (a) Simplified tectonic framework of the Tibetan–Himalayan orogen (adapted from [10]; the position of the Ailaoshan–Jinshajiang Cenozoic alkali-rich porphyry belt is adapted from [85]); (b) Spatial distribution of Cenozoic porphyry and Tertiary basin in the eastern Tibetan–Himalayan orogen (adapted from [73]); (c) Simplified geological map of Cenozoic Yulong porphyry (adapted from [13]).

[17,18]. The phlogopite–garnet clinopyroxenite consists mainly of Ca-rich clinopyroxene (40–60%), garnet (20–50%) and mica (~10%) with a medium- to coarse-grained texture [18]. Detailed mineral chemistry indicates that such a xenoliths were originated from the mantle at the depth of 87–95 km [18].

The YP includes two relatively large intrusive bodies, which intruded into the Late Triassic carbonates and clastic rocks (Fig. 1c). Liang [19] reported the SHRIMP U–Pb zircon age for the largest intrusive body with the result of 40.9 ± 0.1 Ma. However, he did not show the detailed analytical data. We have carried out SHRIMP U–Pb zircon dating for another relatively large intrusive body, and obtained an age of 38.9 ± 0.8 Ma (see below).

Contemporaneous volcanic rocks are all alkali-rich and typically erupted in the strike-slip pull-apart basins. The volcanic rocks in the Nangqen basin, including trachyte, latite, shoshonite, tephrite, tephriphonolite and phonotephrite, erupted at about 38.7 Ma (^{40}Ar–^{39}Ar plagioclase age; [20]). These volcanic rocks belong to shoshonitic series and were inferred by [21] to be derived by partial melting of an enriched mantle source.

2.2. Petrography of the YP

According to Q'-ANOR classification [22], monzogranite-porphyry is the main rock type, with minor syenogranite-, alkali–feldspar granite- and quartz monzonite-porphyries. These are light grey to light purplish-red with a typical porphyritic texture. The phenocrysts (mostly 5–10 mm, ~40%) include plagioclase, amphibole, biotite, alkali feldspar, quartz and minor pyroxene (Fig. 2). Plagioclase phenocryst shows typical normal zoning. Some quartz phenocryst has a resorption texture (Fig. 2b) and the pyroxene phenocryst shows partial melting texture (Fig. 2c), which implies that they probably represent the early-crystallized minerals. Such quartz phenocrysts contain melt inclusions [14]. The matrix consists of alkali feldspar, plagioclase, quartz, amphibole and biotite, with a fine-grained (mostly 0.2–0.5 mm) granitic texture. The porphyry has abundant accessory minerals, including magnetite,

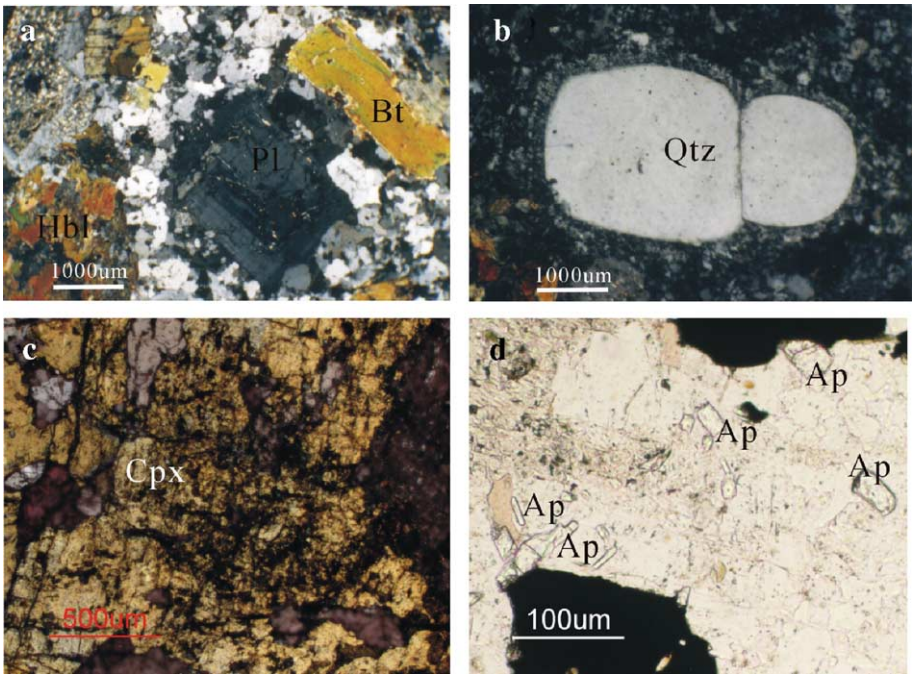

Fig. 2. Photomicrographs of the YP. Pl=plagioclase, Bt=biotite, Hbl=amphibole, Cpx=clinopyroxene, Qtz=quartz, Ap=apatite.

apatite (Fig. 2d), sphene, zircon, allanite, and rutile. In addition, picotite and chromite, which are the characteristic minerals in ultramafic rocks, are also found in the porphyry [13], suggesting some genetic link to the mantle source.

3. Sampling and analytical methods

Thirty samples from prospecting trench and surface exposures have been collected and the sample locations are shown in Fig. 1c. After petrographic examination, the freshest 18 samples were selected for mineral chemical and whole-rock geochemical analyses.

Electron microprobe analysis has been carried out on biotite, amphibole, pyroxene, plagioclase, and K-feldspar, using a JEOL JXA-8800 Superprobe at the State Key Laboratory for Mineral Deposits Research in Nanjing University. Operating conditions were 15 kV at 10 nA beam current. For amphibole, pyroxene and biotite, the standards used were hornblende (for Si, Ti, Al, Fe, Ca, Mg, Na and K) and fayalite (for Mn). For feldspar, the standards used were hornblende (for Si, Ti, Al, Fe, Ca and Mg), albite (for Na), orthoclase (for K) and fayalite (for Mn).

Whole rock chemistry was determined at the Center of Modern Analysis, Nanjing University by XRF for major elements with the precision better than 5%, and at the State Key Laboratory for Mineral Deposits Research, Nanjing University by a Finnigan Element II ICP-MS for trace elements with the precision better than 8%. Detailed analytical procedures for trace elements are described by [23]. Sr and Nd isotopic compositions were measured in the Open Laboratory for Isotope Geology of the Chinese Academy of Geological Sciences, following the methods of [24]. $^{87}Sr/^{86}Sr$ and $^{143}Nd/^{144}Nd$ ratios are reported as measured, and normalized to $^{86}Sr/^{88}Sr$ of 0.1194 for Sr and to $^{146}Nd/^{144}Nd$ of 0.7219 for Nd. During the period of analysis, measurements for the Johnson Matthey Nd_2O_3 standard yield result of $^{143}Nd/^{144}Nd$ ratio of 0.511126 ± 9 (2σ, $n=27$), and for NBS-987 Sr standard yield result of $^{87}Sr/^{86}Sr$ ratio of 0.710228 ± 14 (2σ, $n=30$). Total analytical blanks were 5×10^{-11} g for Sm and Nd and $(2–5) \times 10^{-10}$ g for Rb and Sr.

Pb isotopic analyses for the feldspar phenocrysts that were separated from 10 porphyry samples, respectively, were carried out at the State Key Laboratory for Mineral Deposits Research, Nanjing University by the following procedures. About 50 mg samples were completely dissolved in HNO_3+HCl. After dried, the residue was redissolved in $HBr+HNO_3$ and loaded into a column with 50 μm of AG 1-X8 anionic resin. The extracted Pb was then purified in a second column. Approximately 100 ng Pb was loaded onto single rhenium filaments using the silica-gel technique [25]. Pb isotope analyses were performed on a Finnigan MAT Triton TI thermal ionizing mass spectrometer (TIMS). Analytical reproducibility of 0.01% (2σ) for

$^{206}Pb/^{204}Pb$, 0.01% for $^{207}Pb/^{204}Pb$ and 0.02% for $^{208}Pb/^{204}Pb$ was attained in this study. Mass fractionation corrections have been made from runs of the NBS-981 standard basing on the value of [26], and the error on the mass fractionation corrections is 0.04%.

The zircons for SHRIMP U–Pb dating were processed through conventional magnetic and heavy liquid separation methods, and then handpicked out under binocular microscope to get pure zircon grains for analysis. The zircon grains were mounted in epoxy, and then polished for subsequent cathodoluminescence (CL) observation and SHRIMP analyses. The CL images were taken at the Electron Microprobe Group of the Institute of Mineral Resources, Chinese Academy of Geological Sciences, and the zircon in situ U–Th–Pb isotope analyses were performed with an SHRIMP-II at the Beijing SHRIMP Center, Institute of Geology of Chinese Academy of Geological Sciences. More detailed mount-making and analytical procedures are described by [27]. The standard TEM zircons (417 Ma) were used in interelement fractionation, and U, Th and Pb concentrations were determined based on the standard Sri Lankan gem zircon SL13 (572 Ma). Data processing was carried out using the SQUID 1.03 and Isoplot/Ex 2.49 programs of [28,29], and the ^{204}Pb-based method of common Pb correction was applied.

In situ Hf isotope analysis of zircons that have been determined SHRIMP U–Pb ages were carried out by means of 193 nm laser attached to Neptune multi-collector ICP-MS (LA-MC-ICPMS) at the Institute of Geology and Geophysics, Chinese Academy of Sciences, using techniques described in detail by [30]. Most LAM analyses were carried out in Ar carrier gas with a beam diameter of 31.5–63 μm, a 6–8 Hz repetition time. For the calculation of ε_{Hf} values we have adopted the chondritic values of [31].

4. Results

4.1. SHRIMP U–Pb zircon dating

SHRIMP U–Pb zircon dating results are summarized in Table A1 in Appendix A and illustrated in Fig. 3. The CL images of zircon demonstrated the grain size mostly between 150 and 250 μm. All the zircons show regular oscillatory magmatic zoning with no resorption cores. U and Th contents of analyzed zircons are of 395–1902 and 271–1615 ppm, respectively, with Th/U ratios ranging from 0.28 to 0.85. These Th/U ratios are higher than those of metamorphic zircons that generally show lower Th/U ratios (<0.1), but consistent with

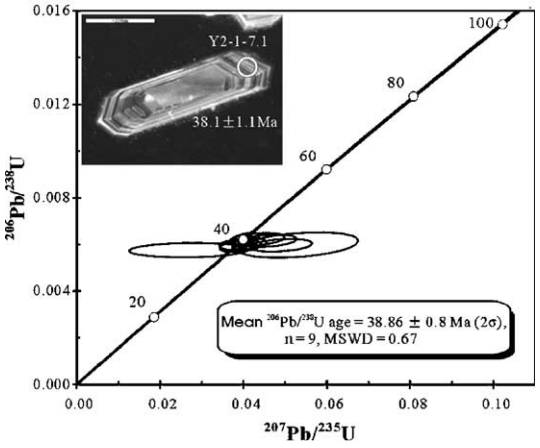

Fig. 3. SHRIMP U–Pb zircon concordant curve. The inset shows a typical CL image of zircon.

those of magmatic zircons [32]. Nine U–Pb analyses show a narrow range of $^{206}Pb/^{238}U$ ages, from 40.0 to 37.0 Ma, plotting in-group on the concordant curve. The concordant curve (Fig. 3) reflects relatively large uncertainties associated with $^{207}Pb/^{235}U$ ages, which may be related to correction of common lead that is difficult to determine precisely. However, this effect is minor for the $^{206}Pb/^{238}U$ ages. Consequently, we quoted $^{206}Pb/^{238}U$ ages to indicate crystallization age of the YP magma. All analyses yield a weighted mean $^{206}Pb/^{238}U$ age of 38.86 ± 0.8 Ma with the MSWD of 0.67 at the 95% confidence interval (2σ).

4.2. Mineral chemistry

4.2.1. Feldspars

Plagioclase phenocryst in the porphyry shows typical normal zoning from andesine (An=30.7–33.4%) in the core to oligoclase (An=22.9–27.4%) at the rim (Table A2 in Appendix A). Plagioclase in the matrix belongs to albite (An=0.5–2.7%) (Table A2). Alkali feldspars in the phorphyry are all sanidine, showing high contents of Or (78.9–91.3%) with minor to medium amounts of Ab (8.7–20.4%) and negligible amounts of An (0–0.7%) (Table A2).

4.2.2. Biotite

The compositions of biotite (phenocryst) are generally characterized by high MgO and low FeO contents with high $Mg/(Mg+Fe^{2+})$ ratios from 0.74 to 0.78 (Table A2). According to the classification of [33] for biotite, the studied biotites belong to iron-phlogopite and eastonite. In addition, the studied biotites have high Fe^{3+}/Fe^{2+} ratios (0.7–1.4). Mg-rich biotite with high Fe^{3+}/Fe^{2+} ratios is typical of shoshonitic rocks [34].

The high Fe^{3+}/Fe^{2+} ratios probably reflect a high Fe^{3+}/Fe^{2+} in the liquids, which may be related to the high fO_2 of the magmas and to their high whole-rock alkali contents, especially K, which stabilize Fe^{3+} over Fe^{2+} at any given fO_2 [34,35]. The biotite in the porphyry also has very high F content, up to 2.3 wt.% [13]. The chemical characteristics of the Yulong biotites are similar to those of biotites in the mantle xenoliths of phlogopite–garnet clinopyroxenite mentioned above (Table A2).

4.2.3. Amphibole

The studied amphibole phenocrysts have high CaO and MgO but low TiO_2 contents (Table A2). According to the classification of [36] for calcic amphibole, a majority of the studied amphibole is edenite and edenitic hornblende, with minor magnesio-hornblende. The amphiboles also have high $Mg/(Mg+Fe^{2+})$ ratios, ranging from 0.61 to 0.70.

The pressure of calcic amphibole crystallization can be estimated using Al-in-hornblende geobarometer [37]:

$$P(\text{kbar}) = -3.46 + 4.23(Al_T)$$

where Al_T is the total number of Al atoms in amphibole per unit formula calculated on the basis of 23 oxygens. The calcic amphiboles in the YP have the appropriate buffering assemblage of horblende+biotite+plagioclase+quartz+sanidine+magnetite [37] and are thus suitable for estimations of crystallization pressure. The results are 1.4–3.0 kbar [average 2.0 kbar (~7 km)], implying the depth of about 7 km for the magma chamber.

4.2.4. Pyroxene

Five different parts (2 for centers and 3 for margins) of a pyroxene phenocryst were analyzed. The results show that the pyroxene has high MgO, intermediate CaO and low Na_2O contents (Table A2), belonging to subcalcic augite (Fig. 4). The centers have higher Al_2O_3 contents than margins (Table A2). Lindsley [38] proposed a graphical thermometer based on experimental data for Ca–Mg–Fe pyroxenes. It is suggested that application be limited to pyroxenes in which Wo+En+Fs exceed 90%. For the pyroxene discussed here, Wo+En+Fs does exceed 90%, and are therefore suitable for the application of this geothermometer. The compositions of the studied pyroxene, using the correction procedure of [39], indicate a high temperature about 1220 °C for a pressure of 10 kbar (Fig. 4).

Experimental studies have shown that Al contents in Ca-rich clinopyroxene increase with increasing crystallization pressure and temperature (e.g. [40]). The calculated pressures and temperatures, using the method of [40], are 1.11–1.22 GPa (37–40 km) and 1259–1271 °C for the centers, and 0.71–0.88 GPa (23–29 km) and 1216–1235 °C for the margins of the studied pyroxene. Therefore, it is most likely that the studied pyroxene represents phenocryst that crystallized during rapid rising of magma from the deep to magma chamber. This, together with a resorption texture for the studied pyroxene phenocryst could imply that the primary magma for the YP had anomalously high temperature (>1200 °C).

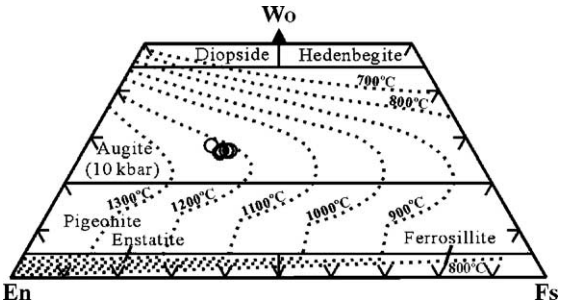

Fig. 4. Pyroxene quadrilateral diagrams [86] with temperature contours for 10kbar pressure from [38]; data plotted using the correction procedure of [39].

4.3. Whole-rock geochemistry

The YP has high SiO_2 (64.8–69.4 wt.%) and Al_2O_3 (15.4–17.0 wt.%) contents. All the samples are peraluminous with values of the alumina saturation index ASI [=molar $Al_2O_3/(CaO+Na_2O+K_2O)$] of 1.02–1.22 (Table A3 in Appendix A). The porphyry shows shoshonitic affinities. The samples are enriched in alkalis (Fig. 5a) and have high K_2O contents (Fig. 5b) with K_2O/Na_2O ratios from 1.0 to 2.7 (most between 1.0 and 1.4). They are strongly enriched in LILE and LREE (Table A3, Figs. 6,7a, b).

The porphyry also shows some affinities with the adakites [6], e.g., high SiO_2 (>56 wt.%) and Al_2O_3 (>15 wt.%), and low MgO (<3 wt.%) contents, depleted in Y (5.1–16 ppm) and Yb (0.53–1.5 ppm), and enrichment in Sr (612–1024 ppm) with high Sr/Y (59–180) and La/Yb (43–73) ratios (Fig. 7c, d), and no Eu anomalies (Fig. 7a).

The geochemical characteristics of the YP are similar to those of acid (SiO_2>63%) compositions of the coeval Nangqen volcanic rocks (NVR), which also show both shoshonitic and adakitic affinities. However, the NVR with intermediate to basic compositions only show shoshonitic affinity. They have much higher LILE and REE concentrations than the YP (Table A3, Figs. 6,7).

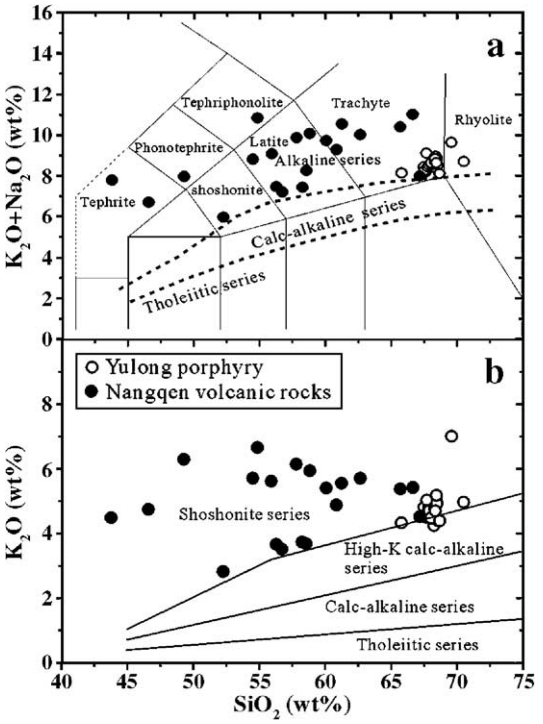

Fig. 5. (K_2O+Na_2O) vs. SiO_2 diagram [87] (a), and K_2O vs. SiO_2 diagram (b) for the YP. The NVR [21] are also plotted for comparison.

The YP shows a narrow range of $\varepsilon_{Nd}(T)$ values (−2.0 to −3.0) (Table A3), similar to that of the NVR (−0.6 to −3.2; [21]). The YP has slightly higher initial $^{87}Sr/^{86}Sr$ ratios (0.7063–0.7070) than the NVR (0.7050–0.7061; [21]). Both the YP and NVR plot in the enriched quadrant of a conventional Sr–Nd isotope diagram (Fig. 8a), where they overlap the field of the Batu Tara (eastern Sunda arc, Indonesia) potassic volcanic rocks [41], but distinguish the Yarlung-Zangbo MORB and adakites related to slab melting and Amdo orthogneiss (a proxy for south Tibet lower crust by [42]) (Fig. 8a). The Nd model ages of the YP relative to depleted mantle (T_{DM}) range from 0.8 to 1.0 Ga (mean 0.9 Ga) (Table A3), which are consistent with those of Miocene potassic volcanic rocks in the Tibetan plateau that have T_{DM} of 0.8–1.3 Ga with an average of 0.9 Ga [9]. Because the Sm/Nd of a melt is generally lower than that of its source, these T_{DM} represent minimum ages of enrichment event and thus most probably Mesoproterozoic metasomatism.

4.4. Feldspar Pb isotope

The Pb isotopic compositions of feldspar phenocrysts show a narrow range of $^{206}Pb/^{204}Pb$ ratios (18.71–18.82) and unusually radiogenic $^{207}Pb/^{204}Pb$ (15.65–15.67) and $^{208}Pb/^{204}Pb$ (38.87–39.00) ratios (Table A3), plotting well above the Northern Hemisphere Reference Line (NHRL; [43]) in conventional Pb isotope diagrams (Fig. 8b). The YP shows similar $^{206}Pb/^{204}Pb$ ratios to the NVR (18.62–18.97; [21]), but has higher $^{207}Pb/^{204}Pb$ ratios than the NVR (15.51–

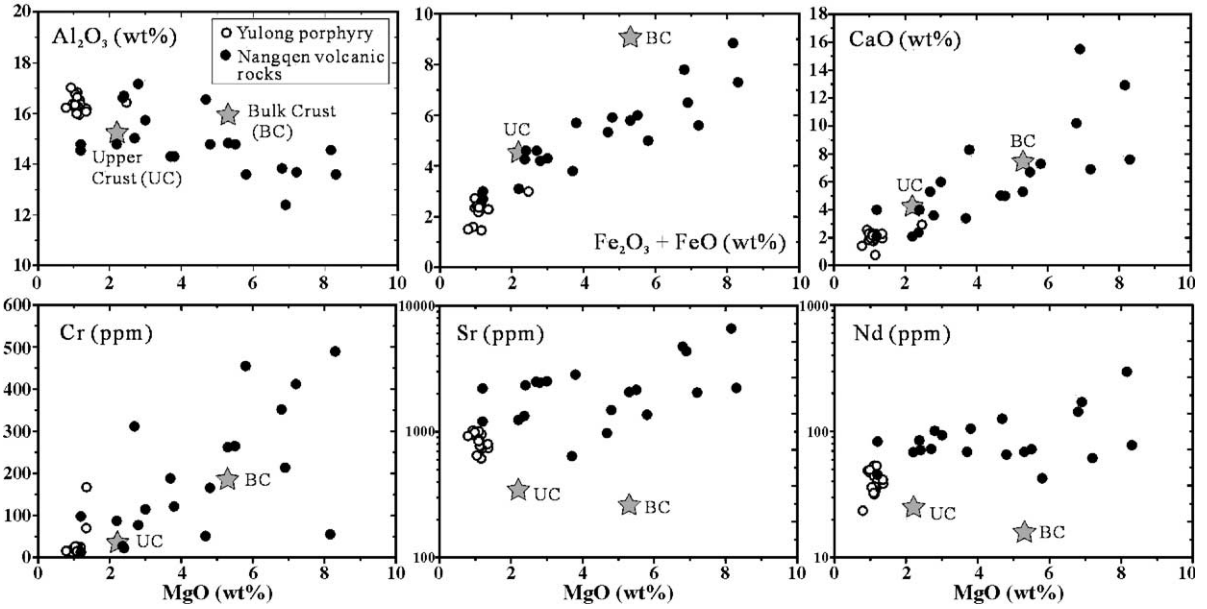

Fig. 6. Selected major element oxides and trace elements against MgO contents. Average major and trace element compositions of the bulk (BC) and upper crust (UC) [53] are also plotted for comparison.

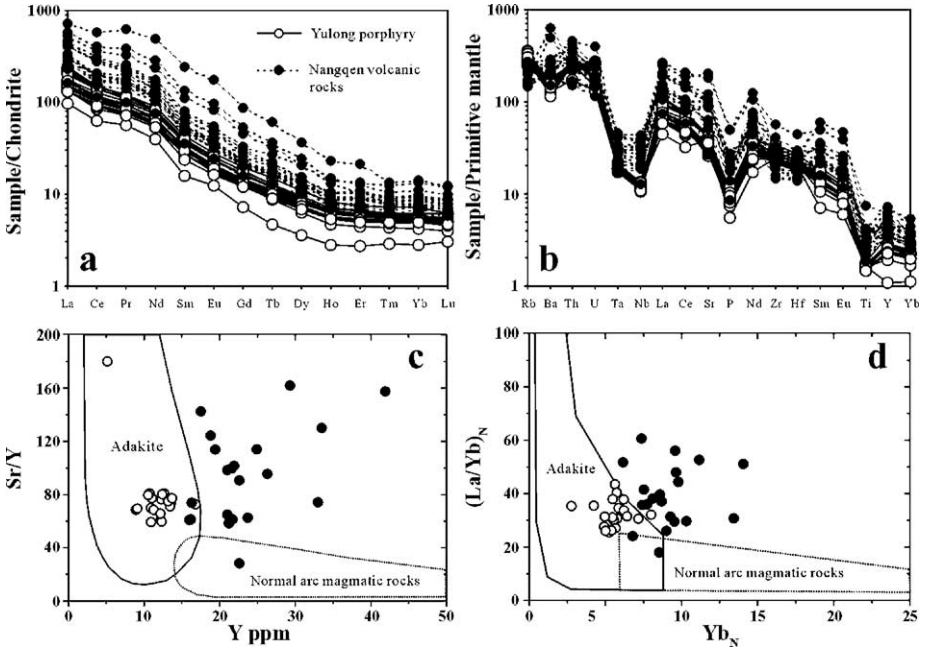

Fig. 7. Chondrite-normalized [88] REE patterns (a), primitive mantle-normalized [89] trace element patterns (b), Sr/Y vs. Y diagram (c), and $(La/Yb)_N$ vs. Yb_N diagram (d) of the YP and NVR. The data of the NVR are from [21].

15.64; [21]) (Fig. 8b). $^{208}Pb/^{204}Pb$ ratios of the YP plot within the upper trend of the NVR (38.43–39.00; [21]) in $^{206}Pb/^{204}Pb$ vs. $^{208}Pb/^{204}Pb$ diagram (not shown). The uniform $^{206}Pb/^{204}Pb$ of both the YP and NVR leads to a vertical array on Fig. 8b, similar to that reported for other post-collisional shoshonitic volcanic rocks from Tibet [9] and for Spanish lamproites [44]. As already pointed out by [44], such a correlation is unlikely to have resulted directly from the closed decay of U, as the range in $^{207}Pb/^{204}Pb$ requires the existence of long-term variation in U/Pb, which should have resulted in a large variation in $^{206}Pb/^{204}Pb$. Note that the Pb isotope signatures of the YP and NVR distinguish those of the Yarlung-Zangbo MORB and adakites related to slab melting (Fig. 8b).

4.5. Zircon Hf isotope

Twenty spots of in situ Hf isotope analysis have been determined on zircons of the sample Y2-1. The results are presented in Table 1. They are characterized by clearly positive initial ε_{Hf} values, ranging from +3.1 to +5.9, most between +4 and +5, except for two spots that have negative initial ε_{Hf} values ranging from −10.3 to −11.0 (Table 1). The positive initial ε_{Hf} values are consistent with long-term depleted mantle source, whereas the negative initial ε_{Hf} values could imply the involvement of crustal components into the mantle source, which is in good agreement with the Nd–Sr isotope compositions of the sample Y2-1 that has $\varepsilon_{Nd}(T)$ value of −2.6 and initial $^{87}Sr/^{86}Sr$ ratio of 0.7069.

5. Discussion

5.1. Origin of the YP

A key question for the YP origin is to explain its shoshonitic and adakitic affinities. The YP shows some geochemical similarities to the contemporaneous NVR in the neighboring area, suggesting some genetic link between their petrogeneses. Accordingly, we choose the NVR for comparison as discussed below.

It has been proposed that the majority of shoshonitic rocks are derived by partial melting of subcontinental lithospheric mantle modified by previous introduction of slab-derived fluids or melts (e.g. [9,34,45,46]). Interaction between such hydrous fluids and mantle can lead to the potassic magma formation as suggested by the experimental data of [47]. These experiments demonstrate that reaction between such a fluid (or melt) and mantle peridotite can produce a hybrid phlogopite pyroxenite; partial melting of such ‘‘hybridized’’ mantle would produce potassic melts.

Adakitic affinity such as the enrichment of Sr and the absence of significant Eu anomalies indicates that the source was plagioclase-free. Depletion of HREEs and Y in adakitic rocks requires melting of a mafic

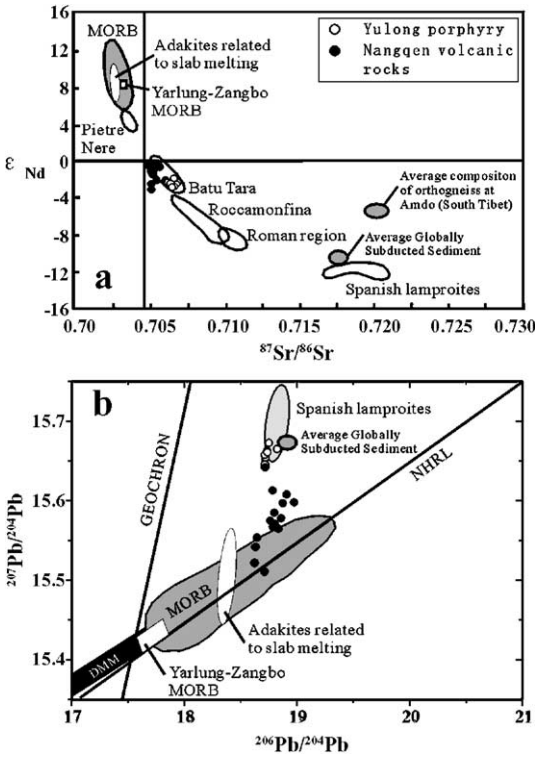

Fig. 8. $^{87}Sr/^{86}Sr$ vs. $^{143}Nd/^{144}Nd$ diagram (a) and $^{207}Pb/^{204}Pb$ vs. $^{206}Pb/^{204}Pb$ diagram (b) showing the isotopic signatures for the YP and related rocks. Pietre Nere, Batu Tara, Roccamonfina, Roman region and Spanish represent orogenic potassic rocks, which plot along a mixing line between an upper mantle end-member having Sr–Nd isotopic compositions similar to MORB, and an enriched mantle end-member having Sr–Nd isotopic compositions similar to those of oceanic sediments [[41] and references therein]. Data for the NVR [21], average composition of globally subducted sediment [59], average composition of Amdo orthogneiss (proxy for Tibet lower crust) [42] are also plotted for comparison. Fields for the Yarlung–Zangbo MORB and adakites related to slab melting are from [[10] and references therein].

source rock within the stability field of garnet, most probably under eclogite-facies conditions [6]. There are at least two possibilities that have been suggested for such a garnet-bearing source to generate the adakitic rocks, i.e., partial melting of subducted oceanic slab (e.g. [6]) and thickened lower crust (e.g. [48]).

5.1.1. Isotopic constraints

Worldwide orogenic potassic magmas such as Batu Tara, Roccamonfina, Roman region and Spanish were proposed to derive from an enriched mantle source associated with slab-derived fluids or melts [[41] and references therein]. Both the YP and NVR plot in the lower right quadrant and within or near the field of Batu Tara potassic rocks (Fig. 8a), indicating that they may have derived from an enriched mantle source associated with earlier slab-derived fluids or melts. The relatively elevated $^{207}Pb/^{204}Pb$ ratios suggest involvement of an old radiogenic component that probably present in the source region as it can be identified in all compositions. The steep trend on the $^{206}Pb/^{204}Pb$ vs. $^{207}Pb/^{204}Pb$ and the shift towards the composition of subducted sediment (Fig. 8b) suggest a component of recycled continent-derived material into the source region.

Of particular interest are the zircon Hf isotopic compositions. The majority of zircons show positive initial ε_{Hf} values, suggesting a depleted mantle source, which contrasts with the enriched mantle source associated with previous subduction-derived fluids inferred by Sr–Nd–Pb isotopic compositions. These decoupled Hf and Sr–Nd–Pb isotopic compositions are most likely to reflect previous subduction process, because HFSE (e.g., Zr, Hf, Nb, Ta) are less soluble than LREE (e.g., La, Ce, Sm, Nd) and LILE (e.g., Rb, Sr, Ba, Pb) in aqueous fluids resulting from dehydration of subducted oceanic crust and sediments (e.g. [49]). However, the few zircons also display pronounced negative initial ε_{Hf} values (-10.3 to -11.0, Table 1). Their unradiogenic Hf at relatively radiogenic Nd [$\varepsilon_{Nd}(T) = -2.6$] isotope compositions, which plots below the mantle array ($\varepsilon_{Hf}=0.33\ \varepsilon_{Nd}+3.19$; [50]), suggests a derivation from a distinctive source. It has been suggested that such distinctive Hf–Nd isotope systematics could be interpreted as being derived from recycled ancient oceanic crust that has been isolated from the convecting mantle for considerable periods of time (>1 Gyr) (e.g. [51]). Accordingly, it is most likely that a lithospheric mantle whose composition has been modified by reaction with ancient (>1 Gyr) slab-derived melts could account for these strongly negative initial ε_{Hf} values of the YP.

In conclusion, the Sr–Nd–Pb–Hf isotopic compositions of the YP and NVR are distinct from MORB, but consistent with the long-term depleted mantle reservoir modified by a subduction-derived components prior partial melting. It is most likely that such a modified mantle source was mainly metasomatized by slab-derived fluid and also hybridized by the addition of small amounts of slab-derived melt.

5.1.2. Partial melting or fractionation?

The YP has similar Sr–Nd isotopic compositions to the contemporaneous NVR. This suggests that the YP could be formed by FC from the mafic magma of NVR. However, their Pb isotopic signature does not support the fractionation model. U/Pb can be enriched in melts as a consequence of the greater incompatibility of U relative to Pb in FC process, which would result in

Table 1
Zircon in situ Hf isotope analysis data of the sample Y2-1 from the YP

Zircon	Spot	$^{176}Lu/^{177}Hf$	$^{176}Hf/^{177}Hf$	$\pm 2\sigma$	$(^{176}Hf/^{177}Hf)_i$	ε_{Hf} (39 Ma)
1	1.1	0.000856	0.282438	0.000043	0.282437	−11.0
2	2.1	0.000779	0.282835	0.000031	0.282834	+3.1
3	3.1	0.000767	0.282857	0.000024	0.282856	+3.8
	3.2	0.000860	0.282856	0.000031	0.282855	+3.8
4	4.1	0.001091	0.282910	0.000025	0.282909	+5.7
6	6.1	0.000684	0.282860	0.000022	0.282860	+4.0
	6.2	0.000704	0.282840	0.000025	0.282839	+3.2
7	7.1	0.000798	0.282878	0.000027	0.282877	+4.6
8	8.1	0.000910	0.282877	0.000023	0.282876	+4.5
9	9.1	0.000608	0.282887	0.000024	0.282887	+4.9
10	10.1	0.000971	0.282881	0.000024	0.282880	+4.7
11	11.1	0.001321	0.282916	0.000019	0.282915	+5.9
12	12.1	0.000878	0.282857	0.000029	0.282856	+3.8
13	13.1	0.000732	0.282456	0.000038	0.282455	−10.3
14	14.1	0.000798	0.282875	0.000028	0.282874	+4.5
15	15.1	0.001309	0.282900	0.000032	0.282899	+5.3
16	16.1	0.001495	0.282904	0.000025	0.282903	+5.5
17	17.1	0.000725	0.282877	0.000025	0.282876	+4.6
18	18.1	0.000779	0.282862	0.000021	0.282861	+4.0
19	19.1	0.000873	0.282874	0.000020	0.282873	+4.4

All the spots are localized at the rim of the zircons; the zircon No. 1 to 10 are corresponding to those of zircons listed in Table A1 in Appendix A that have been determined SHRIMP U–Pb ages.

elevation of both $^{207}Pb/^{204}Pb$ and $^{206}Pb/^{204}Pb$ ratios. Although the YP has higher $^{207}Pb/^{204}Pb$ ratios than the NVR, their near-vertical array of $^{207}Pb/^{204}Pb$ against $^{206}Pb/^{204}Pb$ (Fig. 8b) rules out the closed-system decay of U. This feature is also unlikely to reflect crustal contamination, as sediments tend to show a broad range in $^{206}Pb/^{204}Pb$. Accordingly, the Pb isotopic signature implies that they must have had a complex multi-stage evolution in the source region, as pointed out by [44]. The positive correlations of CaO, total Fe (Fe_2O_3+FeO) and Cr vs. MgO and negative correlation of Al_2O_3 vs. MgO (Fig. 6) could reflect clinopyroxene-dominated fractionation. However, La/Yb ratios do not remain constant with La increase predicted by FC (Fig. 9a). In addition, the La/Yb ratios are uncorrelated with Mg# (not shown), which does also not reflect FC or AFC. In fact, both the YP and NVR show a relatively steep trend of La against La/Yb (Fig. 9a), most probably reflecting a partial melting model.

Adakitic magmas, whether derived directly from partial melting of the subducted oceanic slab (MORB) or from lower crustal mafic rocks, usually show characteristics of low Mg (Mg# <0.44) and high Na_2O (>4.3 wt.%) rather than high K_2O, as demonstrated by experimental studies [52]. The Sr–Nd–Pb–Hf isotopic compositions of the YP that are distinct from MORB, together with its high Mg# (0.50–0.67) and high K_2O contents (4.2–6.9 wt.%) (Table A3), require that if the magma originated by slab melting, it must have experienced significant crustal assimilation, or melt/peridotite interaction, or binary melt mixing. Crustal contamination could increase K_2O contents but could not increase Mg#. Moreover, there is no correlation ($r=-0.36$) between initial $^{87}Sr/^{86}Sr$ ratios and Rb contents in the YP, as would be expected if the high $^{87}Sr/^{86}Sr$ results from assimilation of high-Rb/Sr crust. The uniform positive initial ε_{Hf} values also rule out the significant crustal assimilation. In fact, the K_2O contents in the YP are higher than those typically observed in the continental upper crust (3.4 wt.%; [53]). The concentrations of incompatible element such as Sr and Nd in the YP are also higher than those typically observed in the continental crust (Fig. 6), and thus make their chemistry insensitive to crustal contamination. Although interaction between the slab melt and enriched mantle (EMII) can increase Mg#, the process cannot result in the increase in the K_2O contents. An alternative possibility is binary mixing between pristine adakitic melts and enriched mantle-derived melts represented by coexisting NVR with high Mg# (0.54–0.79). However, the YP has similar K_2O contents and Sr–Nd isotopic compositions to the NVR, which is against the mixing model. Although Pb isotopic compositions of the YP and NVR show a mixing trend (Fig. 8b), $^{207}Pb/^{204}Pb$ ratios for the YP should be lower than those for the NVR as the mixing model expected,

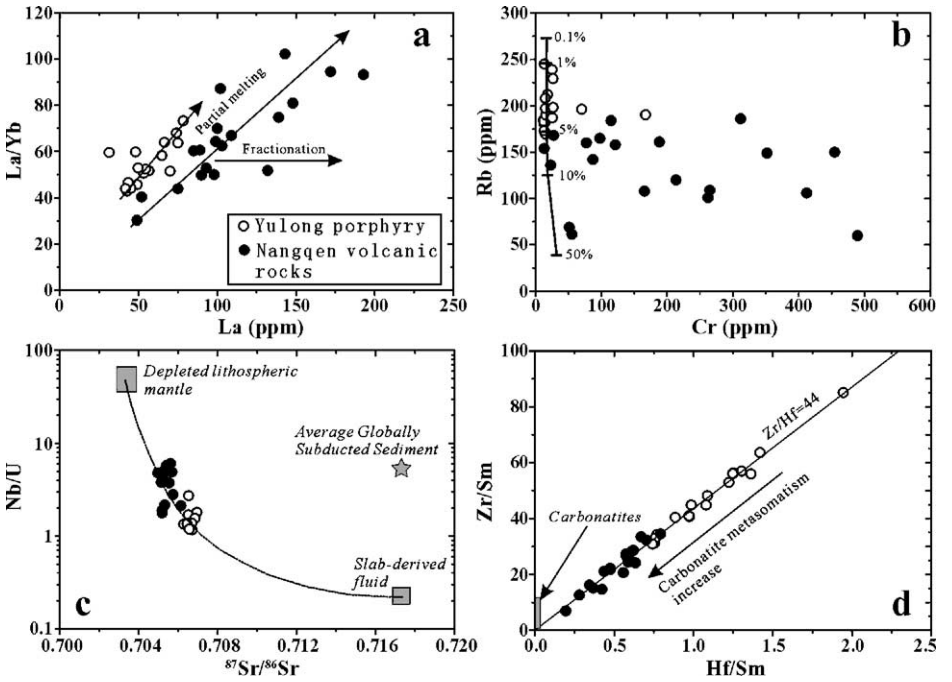

Fig. 9. La/Yb vs. La (a), Rb vs. Cr (b), Nb/U vs. $^{87}Sr/^{86}Sr$ (c), and Zr/Sm vs. Hf/Sm (d) diagrams for the YP. Data for the NVR [21] are also plotted for comparison. In (b), curve shown is for batch modal melting (percent melting indicated) of a mafic source with 21 ppm Rb and 562 ppm Cr, equivalent to the mantle xenoliths of phlogopite–garnet clinopyroxenite [17], with residue of 0.50 clinopyroxene, 0.45 garnet and 0.05 phlogopite. Mineral/melt partition coefficients are from [54,90]. In (c), data for globally subducted sediment and slab-derived fluid are from [59] and [60], respectively. In (d), the field for carbonatites is from [67].

which is also opposite to observation. Furthermore, the scatter of Mg# vs. La/Yb does not support the significant mixing process. Similarly, the features mentioned above can rule out the possibility that the YP was derived from partial melting of the thickened lower crustal mafic rocks, plus additional input from an enriched mantle represented by coexisting NVR or an upper crustal source. The YP also could not formed by AFC process of the Nangqen shoshonitic magma due to their similar Sr–Nd isotopic compositions.

To sum up, we consider that the effects of FC and AFC as well as magma mixing are not important in the YP origin. The most plausible explanation is that the YP was derived directly by partial melting of an enriched lithospheric mantle as the shoshonitic NVR did. Such an enriched mantle was a subduction-modified source as inferred by Sr–Nd–Pb–Hf isotopic signatures mentioned above and further discussed below. To further evaluate the partial melting model, we use a plot of Cr against Rb (Fig. 9b). For a source that leaves pyroxene or garnet in the residue, Cr should be a strongly compatible element and Rb an incompatible element [54]. Consequently, Cr should exhibit much less variation than Rb for low to moderate degrees (<50%) of partial melting. Fig. 9b illustrates that the majority of the YP and acid NVR show a narrow arrange of Cr with a wide variation of Rb, fitting a partial melting model for a mafic source such as phlogopite–garnet clinopyroxenite. However, the intermediate to basic NVR has high Cr abundance, precluding mafic rocks as a potential source.

5.1.3. Evidence for phlogopite in the source region

Both the YP and NVR have high K_2O contents, forming a relatively flat array of K_2O against SiO_2 (Fig. 5b). Such a flat array suggests buffering of a potassic phase such as phlogopite, potassic amphibole or K-feldspar in the source region. The absence of significant Eu anomalies of the YP and NVR (Fig. 7a) rules out K-feldspar as a potassic phase. The positive correlation between the La concentrations and La/K ratios (not shown) further supports that a potassic phase of phlogopite or potassic amphibole is present in the mantle source region [35]. Furman and Graham [55] suggested that melts in equilibrium with phlogopite be expected to have significantly higher Rb/Sr (>0.1) and lower Ba/Rb (<20) ratios than those (Rb/Sr<0.06, Ba/Rb>20, respectively) formed from amphibole-bearing mantle sources. The YP and most NVR have high Rb/Sr (>0.06) and low Ba/Rb (<20) ratios, strongly

suggesting phlogopite rather than potassic amphibole as the main potassic phase.

5.1.4. Evidence for subduction-modified mantle

The YP is enriched in LILE. The absolute concentrations of many trace elements (e.g. Sr) are higher than typically observed in the continental crust (Fig. 6). The silicate fluid metasomatism in the mantle source, which involved the formation of phlogopite, could account for such enrichment, as has been suggested that phlogopite is the major repositories for these elements in lithospheric mantle (e.g. [56]). The depletion of HFSE relative to its neighboring element in the primitive mantle normalized patterns such as negative Nb–Ta and Ti anomalies (Fig. 7b) is recognized as a fingerprint of subduction process (e.g. [57]). The Nb/U ratios (1.2–2.7) of the YP are significantly lower than that of MORB and ocean island basalt (OIB) (47; [58]), and also lower than estimates for the continental crust (upper crust Nb/U ≈ 9; [53]) and average composition of globally subducted sediment (Nb/U ≈ 5; [59]). Therefore, nonmagmatic enrichment in the source region is required, given the general awareness that igneous processes in the mantle have a minimal effect on fractionating this elemental ratio [58]. These significantly lower Nb/U ratios (1.2–2.7) are close to that calculated for subduction-zone fluids (Nb/U ≈ 0.22; [60]). This has been generally ascribed to the strong capacity of LILE and the inability to transfer significant amounts of HFSE in the slab-derived hydrous fluid. The HFSE are more likely to be stored in phases such as rutile and/or ilmenite, which may persist in the subducted slab [61]. Accordingly, such a slab-derived hydrous fluid could account for the low Nb/U ratios of the YP. On Nb/U against $^{87}Sr/^{86}Sr$ (Fig. 9c), the YP plots close to the mixing curve between the slab-derived fluid and depleted lithospheric mantle source. The NVR show higher Nb/U ratios and lower $^{87}Sr/^{86}Sr$ ratios than the YP (Fig. 9c), suggesting less proportion of slab-derived components in their source region.

It is also worthy to discuss the sub-chondritic Nb/Ta ratios (8.6–12.0, Table A3) for the YP. Both Nb and Ta show similar geochemical behaviors due to their nearly identical ionic radii and charge [62], so Nb/Ta ratio is hardly affected by magmatic processes such as fractional crystallization and partial melting. Indeed, MORB vary little in Nb/Ta ratio and their average ratio of 16.7 is indistinguishable from the primitive mantle value of 17.4 [63]. The Nb/Ta ratio of the Cenozoic adakites formed by direct melting of subducted oceanic crust is similar to that of MORB [64]. The YP has lower Nb/Ta ratios than MORB, which suggests that nonmagmatic enrichment in the source region is required. A review of the geochemical literature [64] confirms that Nb/Ta represents element pair with similar MORB melting partition coefficient but different fluid/solid partition coefficient, which results in lower Nb/Ta ratio of arc melts from hydrated mantle wedge peridotite than that of direct slab melts. Accordingly, the lower Nb/Ta ratios of the YP also suggest that the mantle source was modified by a slab-derived hydrous fluid.

5.1.5. Evidence for carbonate metasomatism

The YP is enriched in REE especially LREE. The absolute concentrations of many trace elements (e.g. Nd) are higher than typically observed in the continental crust (Fig. 6). The NVR show higher REE concentrations than the YP (Fig. 7a). It has been suggested that carbonate metasomatism may be responsible for the commonly observed REE especially LREE enrichment of the depleted lithospheric mantle [65], because of high REE contents of mantle-derived carbonatite with Ce equal to ~600 times chondrite and Yb equal to ~15 times chondrite [66]. Both the YP and NVR show higher Zr/Hf ratios (around 44, Fig. 9d) and lower Ti/Eu (Fig. 7b). Such Zr/Hf and HFSE/REE fractionations have also been attributed to the carbonate metasomatism in the mantle source (e.g. [66,67]). The Zr/Sm ratio is positively correlated with the Hf/Sm ratio (Fig. 9d). This linear correlation with its orientation toward the field of carbonatites suggests that variations of abundance ratios involving Zr, Hf, and Sm in the mantle source are dominated by carbonates, perhaps reflecting variable intensity of metasomatism by carbonate-rich fluids [67]. The NVR show lower Zr/Sm and Hf/Sm ratios than the YP (Fig. 9d). This, together with the higher contents of Ba, Sr, and REE for the NVR and with the highest abundance of these elements and lowest ratios of Zr/Sm and Hf/Sm for the most silica-undersaturated rocks (tephrite), suggests that the carbonate metasomatism in the source region was more intensive for the NVR than for the YP. The carbonate metasomatism in the mantle source would produce clinopyroxene, apatite and monazite [66]. Such a clinopyroxene has high CaO and high Mg# and low Al_2O_3 (most between 0.5 and 2.0 wt.%) [66], because the only major element added in significant quantities as a result of the carbonate metasomatism is CaO. However, the clinopyroxene in the pyroxenite veins associated with the silicate fluid or melt metasomatism is characterized by Fe-enrichment and a general addition of Al and Ca [66]. The majority of clinopyroxene in the mantle xenoliths of phlogopite–garnet clinopyroxenite men-

tioned above have high CaO (22.0–24.1 wt.%) and high Mg# (0.70–0.85) and low Al_2O_3 (1.1–2.4 wt.%) [17,18], suggesting the products of carbonate metasomatism for these clinopyroxenes. Only a few clinopyroxenes in phlogopite–garnet clinopyroxenite show lower CaO (10.8–17.5 wt.%) and lower Mg# (0.65–0.69) and higher Al_2O_3 (6.6–7.2 wt.%) [17,18], which is most probably consistent with silicate fluid or melt metasomatism. The apatite, as the product of carbonate metasomatism, is characterized by F-rich and Cl-poor [66]. The abundant apatite (Fig. 2d) in the YP is also enriched in F (2.43–2.73 wt.%) and relatively depleted in Cl (0.08–0.10 wt.%) [13], suggesting some genetic link to the mantle carbonate metasomatism. Thus, as pointed out by [66], carbonate metasomatism should be considered in addition to silicate fluid metasomatism in evaluating the origins of incompatible element enrichments in the lithospheric mantle.

It has been suggested that the carbonate fluid could be derived from the subducted oceanic crust (the overlying marine carbonates) (e.g. [68]). Metasomatism of a depleted mantle by such a carbonate fluid would result in Nb depletion relative to La, in contrast to the Nb enrichment resulting from an asthenosphere-derived carbonate fluid (melt) metasomatism [66]. The YP and NVR show Nb depletions relative to La (Fig. 7b), together with their relative uniform enriched mantle Sr–Nb isotopic compositions (Fig. 8a), suggesting that the associated carbonate fluid was most probably derived from the subducted oceanic crust, like the silicate fluid did.

5.1.6. Nature of the magma source region

Amphibole, phlogopite and carbonate are common metasomatic volatile-bearing phases in the metasomatized mantle (e.g. [56]). A series of experimental studies (e.g. [69]) indicated that the phlogopite–carbonate assemblage with the absence amphibole phase could constraint the source depth to >100 km. This places the source of the Yulong and Nangqen igneous rocks within the lithospheric mantle, because it is expected the crust thickness of ~70 km and lithosphere thickness of >200 km caused by the India-Asia continental collision since the Paleocene [9].

The consensus view is that potassic and ultra-potassic rocks are derived by partial melting of metasomatic veins within an lherzolitic or harzburgitic lithosphere (e.g. [70]). Foley [70] introduced his vein-plus-wallrock melting model for the origin of ultra-potassic as well as potassic rocks. The composition of melts derived from veins is controlled by the degree of partial melting and the relative contributions of vein and wall-rock material. As mentioned above, the vein mineral components for the YP origin are most likely phlogopite (the product of silicate fluid metasomatism), garnet (inferred by adakitic affinity, the product of silicate melt metasomatism [71]), clinopyroxene (the main products of carbonate fluid metasomatism) and minor apatite and carbonate. This is in good agreement with the mineralogy of mantle xenoliths such as phlogopite–garnet clinopyroxenite hosted by alkali-rich porphyry in the neighboring area [17,18]. A plot of Cr against Rb (Fig. 9b) shows that low degree (1–5%) partial melting of such a metasomatic vein, equivalent to the mantle xenoliths of phlogopite–garnet clinopyroxenite with Cr of 562 ppm and Rb of 21 ppm [17], could account for the YP origin. The NVR show higher Cr and lower Rb contents (Fig. 9b), which implies that the wall-rock material (lherzolite) might be involved in partial melting for their origin. This is further supported by the relatively higher proportions of depleted lithospheric mantle compositions for the NVR than for the YP inferred by Sr–Nd–Pb isotopic and elemental compositions (Figs. 8,9c).

5.1.7. What triggered the melting of the metasomatized lithospheric mantle?

The source depth for the YP as well as NVR may be at least 100 km inferred by the volatile phase relations. The early crystallized clinopyroxene geothermometry of the YP indicates that the primary magmas had anomalously high temperature (1220 °C), which is in broad agreement with the homogenization temperatures of melt inclusions hosted by the early crystallized quartz phenocrysts in the YP, ranging from 1000 to >1200 °C ($n=61$), most ($n=48$) between 1150 and 1200 °C [14]. What mechanism is suitable for attainment of such high temperatures to induce partial melting of the metasomatized lithospheric mantle at the depth of 100 km? The YP emplacement (41–39 Ma) and the NVR eruption (39 Ma) post-date the India-Asia continental collision (at about 65 Ma; [72]). This delay would not be expected if fluid release accompanying oceanic or continental subduction was the trigger. It has been suggested a response to convective thinning of the lithosphere for the potassic magmatism (~20 Ma) in the northern and southern Tibetan plateau [9], which triggered a temperature increase in the lithosphere. However, the potassic magmatism of Yulong and Nangqen in the eastern Tibetan plateau pre-dates that in the northern and southern Tibetan plateau. Recently, Hou et al. [73] realized that in the eastern Tibetan plateau, a regional-scale strike-slip fault system caused by the India-Asia continental collision controlled the distribu-

tion of Cenozoic (49–30 Ma) porphyries. Rather, seismic profiles across the Qiangtang terrane indicate that the strike-slip faults are translithospheric and accommodated local mantle uplift with the Moho rising about 2 to 3 km relative to the surrounding area [14,74]. This suggests that these faults most likely caused the upwelling of asthenosphere in the area, which triggered the melting of the metasomatized lithospheric mantle. Such a model is similar to the situation proposed by [75] to interpret the petrogenesis of high-K calc-alkaline and alkaline granites in Central Hoggar (Algeria) during the Pan-African orogeny.

The exotic lithosphere model [76] is another alternative trigger mechanism for partial melting of the metasomatized lithospheric mantle. This model suggests that the India-Asia continental collision results in extrusion of the lithosphere beneath the eastern Tibet to the east beneath the Yangtze craton at 50–40 Ma, which offers an efficient way to thin the lithosphere in this region and therefore triggers the melting of the metasomatized lithospheric mantle.

5.2. Implications for granite and adakite geneses

Nearly 50 years after [77], the origins of granitic magmas remain subjects of debate, disagreement, and study. While it is generally accepted that strongly peraluminous magmas originate by partial melting of micaceous metasedimentary rocks (e.g. [78]), diverse origins are proposed for the more abundant metaluminous-to-weakly peraluminous silicic magmas. Explanations include crystallization-differentiation of basaltic parents (e.g. [79]), partial remelting of igneous rocks [78], assimilation of sialic rocks into differentiating basaltic magmas [80], and partial melting of immature volcanogenic sediments with igneous-like compositions (some metagreywackes [81]). This contribution gives a case study that granite can be derived directly by partial melting of lithospheric mantle. It is, therefore, important to understand the source and origin of diverse granites.

Adakite was proposed over a decade ago to be products of the melting of young subducted oceanic crust related to incipient subduction [6]. Its research has received widespread attention due to its close relation to porphyry copper deposits [82], and many other models for adakite generation have been proposed, such as partial melting of basaltic lower crust (e.g. [48]) or of delaminated lower crust [83] and AFC processes [84]. Adakite formed by these processes usually shows characteristics of low Mg and high Na rather than high K, as demonstrated by experimental studies [52]. However, many adakitic rocks especially in continental collision setting, showing some features of typical adakite in arc settings, also have much higher K_2O contents (e.g. [10]). The mechanism responsible for such K-enrichment in adakite is poorly understood. This contribution indicates that some potassic rocks showing adakitic affinities especially in continental collision environments such as Yulong could have been derived directly by low-degree melting of the phlogopite–garnet clinopyroxenite that was mainly produced by the silicate–carbonate fluid metasomatism in an lherzolitic or harzburgitic lithosphere, whereas most adakites in arc settings was derived by partial melting of the amphibole eclogite and/or garnet amphibolite transformed by a basaltic source of subducted oceanic crust, which is helpful to further understand the geneses of adakite and its associated porphyry deposits.

6. Concluding remarks

The Cenozoic (41–39 Ma) YP is shoshonitic and shows some affinities with the adakite. Detailed elemental and isotopic data suggest that the YP was derived directly by low degree (1–5%) partial melting of the phlogopite–garnet clinopyroxenite that was produced by the slab-derived silicate–carbonate fluid metasomatism and by addition of small amounts of slab-derived melt hybridization at Mesoproterozoic age in an lherzolitic lithosphere at a depth of >100 km. A regional-scale strike-slip fault system and/or an extrusion of the lithosphere to the east caused by the India-Asia continental collision triggered the melting of the metasomatized lithospheric mantle. These anomalously high temperature (>1200 °C) melts rose rapidly and assembled at depths of ~7 km to form a magma chamber, which subsequently was emplaced into Triassic strata to form the shallow-seated YP. This is important to further understand the source and origin of diverse granites and the geneses of porphyry deposits especially in continental collision settings.

Acknowledgments

We are grateful to S.H. Tang from the Isotope Geochemistry Laboratory of the Chinese Academy of Geological Sciences for her assistance with measurements of Nd and Sr isotope compositions, and to L.W. Xie from the Institute of Geology and Geophysics, Chinese Academy of Sciences for his assistance with zircon in situ Hf isotope analysis. Constructive criticisms by three anonymous reviewers and editorial comments by Scott King are acknowledged. This work was finan-

cially supported by the National Key Basic Research Projects (2002CB412603) and the National Natural Science Foundation (40221301).

Appendix A. Supplementary data

Supplementary data associated with this article can be found, in the online version, at doi:10.1016/j.epsl.2005.11.023 [91].

References

[1] D.J. DePaolo, Neodymium isotopes in the Colorado Front Range and crust–mantle evolution in the Proterozoic, Nature 291 (1981) 193–196.
[2] P. Holden, A.N. Halliday, W.E. Stepens, Neodymium and strontium isotope content of microdiorite enclaves points to mantle input to granitoid production, Nature 330 (1987) 53–56.
[3] W. Hildreth, S. Moorbath, Crustal contributions to arc magmatism in the Andes of central Chile, Contrib. Mineral. Petrol. 98 (1988) 455–489.
[4] W.J. Collins, Evaluation of petrogenetic models for Lachlan Fold Belt granitoids: implications for crustal architecture and tectonic models, Aust. J. Earth Sci. 45 (1998) 483–500.
[5] D. Snyder, S. Tait, The imprint of basalt on the geochemistry of silicic magmas, Earth Planet. Sci. Lett. 160 (1998) 433–445.
[6] M.J. Defant, M.S. Drummond, Derivation of some modern arc magmas by melting of young subducted lithosphere, Nature 347 (1990) 662–665.
[7] H. Martina, R.H. Smithiesb, R. Rappc, J.F. Moyend, D. Champione, An overview of adakite, tonalite–trondhjemite–granodiorite (TTG), and sanukitoid: relationships and some implications for crustal evolution, Lithos 79 (2005) 1–24.
[8] K.C. Condie, TTGs and adakites: are they both slab melts?, Lithos 80 (2005) 33–44.
[9] S. Turner, N. Arnaud, J. Liu, Post-collision shoshonitic volcanism on the Tibetan plateau: implications for convective thinning of the lithosphere and the source of ocean island basalts, J. Petrol. 37 (1996) 45–71.
[10] Z.Q. Hou, Y.F. Gao, X.M. Qu, Z.Y. Rui, X.X. Mo, Origin of adakitic intrusives generated during mid-Miocene east–west extension in southern Tibet, Earth Planet. Sci. Lett. 220 (2004) 139–155.
[11] R.H. Xu, U. Scharer, C.J. Allegre, Magmatism and metamorphism in the Lhasa block (Tibet): a geochronological study, J. Geol. 93 (1985) 41–57.
[12] N.B.W. Harris, S. Inger, R. Xu, Cretaceous plutonism in Central Tibet: an example of post-collision magmatism? J. Volcanol. Geotherm. Res. 44 (1990) 21–32.
[13] H.W. Ma, Granitoid and Mineralization of the Yulong Porphyry Copper Belt in Eastern Tibet, China University of Geosciences Publishing House, Bejing, 1990 (157 pp., in Chinese with English abstract).
[14] R.L. Tang, H.S. Luo, The Geology of Yulong Porphyry Copper (Molybdenum) Ore Belt, Xizang (Tibet), China University of Geosciences Publishing House, Bejing, 1995 (320 pp., in Chinese with English abstract).
[15] Z.Q. Hou, X.X. Mo, Y.F. Gao, X.M. Qu, X.J. Meng, Adakite, a possible host rock for porphyry copper deposits: case studies of porphyry copper belts in Tibetan plateau and Northern Chile, Mineral Deposits 22 (2003) 1–12 (in Chinese with English abstract).
[16] X.X. Mo, J.F. Deng, F.L. Dong, Volcanic petrotectonic assemblages in Sanjiang orogenic belt, SW China and implication for tectonics, Geol. J. Chin. Univ. 7 (2001) 121–138 (in Chinese with English abstract).
[17] X.F. Liu, J.D. Liu, C.J. Zhang, D.C. Wu, Y.G. Li, J.D. Li, Z.X. Yang, Study on elemental geochemistry of ultramafic deep xenoliths in alkali-rich porphyry, J. Mineral. Petrol. 23 (2003) 39–43 (in Chinese with English abstract).
[18] X. Zhao, X.X. Mo, X.H. Yu, B.X. Li, J. Zhang, Mineralogical characteristics and petrogenesis of deep-derived xenoliths in Cenozoic syenite-porphyry in Liuhe, western Yunnan, Earth Sci. Front. 10 (2003) 94–104 (in Chinese with English abstract).
[19] H.Y. Liang, New progress of studies on rock-forming and ore-forming processes of porphyry copper deposits in the Southeastern Qinghai-Tibet plateau, Miner. Depos. 21 (2002) 365, (in Chinese).
[20] G.T. Pan, Tectonic Evolution of the Qinghai-Tibet plateau, Geological Publishing House, Beijing, 1990 (243 pp., in Chinese with English abstract).
[21] W.M. Deng, H.J. Sun, Y.Q. Zhang, Petrogenesis of Cenozoic potassic volcanic rocks in Nangqen Basin, Chin. J. Geol. 36 (2001) 304–318 (in Chinese with English abstract).
[22] A. Streckeisen, R.W. Le Maitre, A chemical approximation to the modal QAPF classification of the igneous rocks, Neues Jahrb. Mineral., Geol. Paläontol., Abh., Abt. A 136 (1979) 169–206.
[23] J.F. Gao, J.J. Lu, M.Y. Lai, Y.P. Lin, W. Pu, Analysis of trace elements in rock samples using HR-ICPMS, J. Nanjing Univ., Nat. Sci. Ed. 39 (2003) 844–850 (in Chinese with English abstract).
[24] Z.Q. Zhang, D.Y. Liu, G.M. Fu, Studying on Isotopic Geochronology of Metamorphic Rock in the Northern Qinling, Geological Publishing House, Beijing, 1994 (232 pp., in Chinese with English abstract).
[25] H. Gerstenberger, G. Haase, A highly effective emitter substance for mass spectrometric Pb isotope ratio determinations, Chem. Geol. 136 (1997) 309–312.
[26] W. Todt, R.A. Cliff, A. Hanser, Evaluation of a ^{202}Pb–^{205}Pb double spike for high-precision lead isotope analysis, Geophys. Monogr. 95 (1996) 429–437.
[27] B. Song, Y.H. Zhang, Y.S. Wan, Mounting and analytical procedure of SHRIMP zircon dating, Geol. Rev. 48 (2002) 26–30 (in Chinese with English abstract).
[28] K.R. Ludwig, Squid 1.02, A User Manual, Berkeley Geochronological Center Special Publication, Berkeley, 2001, pp. 1–219.
[29] K.R. Ludwig, Using Isoplot/EX, version 2.49, A Geolocronological Toolkit for Microsoft Excel, Berkeley Geochronological Center Special Publication, Berkeley, 2001, pp. 1–55.
[30] P. Xu, F.Y. Wu, L.W. Xie, Y.H. Yang, Hf isotopic compositions of the standard zircons for U–Pb dating, Chin. Sci. Bull. 49 (2004) 1642–1648.
[31] J. Blichert-Toft, F. Albarede, The Lu–Hf isotope geochemistry of chondrites and the evolution of the mantle–crust system, Earth Planet. Sci. Lett. 148 (1997) 243–258.
[32] I.S. Williams, A. Buick, I. Cartwright, An extended episode of early Mesoproterozoic metamorphic fluid flow in the Reynold Region, central Australia, J. Metamorph. Geol. 14 (1996) 29–47.

[33] M.D. Foster, Interpretation of the composition of trioctahedral mica, U. S. Geol. Surv. Prof. Pap. 354-B (1960) 11–48.
[34] Y.H. Jiang, S.Y. Jiang, H.F. Ling, X.R. Zhou, X.J. Rui, W.Z. Yang, Petrology and geochemistry of shoshonitic plutons from the western Kunlun orogenic belt. China: implications for granitoid geneses, Lithos 63 (2002) 165–187.
[35] S.N. Feldstein, R.A. Lange, Pliocene potassic magmas from the Kings River region, Sierra Nevada, California: evidence for melting of a subduction-modified mantle, J. Petrol. 40 (1999) 1301–1320.
[36] B.E. Leake, Nomenclature of amphiboles, Mineral. Mag. 42 (1978) 533–563.
[37] M.C. Johnson, M.J. Rutherford, Experimental calibration of the aluminum-in-hornblende geobarometer with application to Long Valley caldera (California) volcanic rocks, Geology 17 (1989) 837–841.
[38] D.H. Lindsley, Pyroxene thermometry, Am. Mineral. 68 (1983) 477–493.
[39] D.H. Lindsley, D.J. Andersen, A two-pyroxene thermometer. Proceedings of the Thirteenth Lunar and Planetary Science Conference, Part 2, J. Geophys. Res. 88 (1983) Supplement A887–906.
[40] R.N. Thompson, Some high pressure pyroxenes, Mineral. Mag. 39 (1974) 768–787.
[41] D.R. Nelson, Isotopic characteristics of potassic rocks: evidence for the involvement of subducted sediments in magma genesis, Lithos 28 (1992) 403–420.
[42] H.M. Williams, S.P. Turner, J.A. Pearce, S.P. Kelley, N.B.W. Harris, Nature of the source regions for post-collisional, potassic magmatism in southern and northern Tibet from geochemical variations and inverse trace element modeling, J. Petrol. 45 (2004) 555–607.
[43] S.R. Hart, A large-scale isotope anomaly in the Southern Hemisphere mantle, Nature 309 (1984) 753–757.
[44] D.R. Nelson, M. McCulloch, S.S. Sun, The origins of ultrapotassic rocks as inferred from Sr, Nd and Pb isotopes, Geochim. Cosmochim. Acta 50 (1986) 231–245.
[45] N.W. Rogers, D. James, S.P. Kelley, The generation of potassic lava from the eastern Virunga province, Rwanda, J. Petrol. 39 (1998) 1223–1247.
[46] Y.H. Jiang, H.F. Ling, S.Y. Jiang, H.H. Fan, W.Z. Shen, N. Pei, Petrogenesis of Late Jurassic peraluminous volcanic complex and its high-Mg potassic quenched enclaves at Xiangshan, southeast China, J. Petrol. 46 (2005) 1121–1154.
[47] P.J. Wyllie, T. Sekine, The formation of mantle phlogopite in subduction zone hybridization, Contrib. Mineral. Petrol. 79 (1982) 375–380.
[48] N. Petford, M. Atherton, Na-rich partial melts from newly underplated basaltic crust: the Cordillera Blanca batholith, Peru, J. Petrol. 37 (1996) 1491–1521.
[49] A. Polat, C. Munker, Hf–Nd isotope evidence for contemporaneous subduction processes in the source of late Archean arc lavas from the Superior Province, Canada, Chem. Geol. 213 (2004) 403–429.
[50] J. Vervoort, P.J. Patchett, J. Blichert-Toft, F. Albarede, Relationships between Lu–Hf and Sm–Nd isotopic systems in the global sedimentary system, Earth Planet. Sci. Lett. 168 (1999) 79–99.
[51] G.M. Nowell, D.G. Pearson, D.R. Bell, R.W. Carlson, C.B. Smith, P.D. Kempton, S.R. Noble, Hf isotope sysematics of Kimberlites and their megacrysts: new constraints on their source regions, J. Petrol. 45 (2004) 1583–1612.
[52] R.P. Rapp, E.B. Watson, Dehydration melting of metabasalt at 8–32 kbar: implications for continental growth and crust–mantle recycling, J. Petrol. 36 (1995) 891–931.
[53] S.R. Taylor, S.M. McLennan, The Continental Crust: Its Composition and Evolution, 1985, Blackwell Scientific, Oxford, pp. 57–72.
[54] R.A. Stern, G.N. Hanson, Archean High-Mg granodiorites: a derivative of light rare element-enriched Monzodiorite of mantle origin, J. Petrol. 32 (1991) 201–238.
[55] T. Furman, D. Graham, Erosion of lithospheric mantle beneath the East African Rift system: geochemical evidence from the Kivu volcanic province, Lithos 48 (1999) 237–262.
[56] D.A. Ionov, S.Y. O'Reilly, W.L. Griffin, Volatile-bearing minerals and lithophile trace elements in the upper mantle, Chem. Geol. 141 (1997) 153–184.
[57] M.F. Thirlwall, T.E. Smith, A.M. Graham, N. Theodorou, P. Hollings, J.P. Davidson, R.J. Arculus, High field strength element anomalies in arc lavas: source or process? J. Petrol. 35 (1994) 819–838.
[58] A.W. Hofmann, K. Jochum, M. Seufert, M. White, Nb and Pb in oceanic basalts: new constraints on mantle evolution, Earth Planet. Sci. Lett. 79 (1986) 33–45.
[59] T. Plank, C.H. Langmuir, The chemical composition of subducting sediment and its consequences for the crust and mantle, Chem. Geol. 145 (1998) 325–394.
[60] J. Ayers, Trace element modeling of aqueous fluid–peridotite interaction in the mantle wedge of subduction zone, Contrib. Mineral. Petrol. 132 (1998) 390–404.
[61] F.J. Ryerson, E.B. Watson, Rutile saturation in magmas: implications for Ti–Nb–Ta depletion in island-arc basalts, Earth Planet. Sci. Lett. 86 (1987) 225–239.
[62] K.P. Jochum, H.M. Seufret, B. Spettel, H. Palme, The solar-system abundances of Nb, Ta, and Y, and the relative abundances of refractory lithophile elements in differentiated planetary bodies, Geochim. Cosmochim. Acta 50 (1986) 1173–1183.
[63] B.S. Kamber, K.D. Collerson, Role of 'hidden' deeply subducted slabs in mantle depletion, Chem. Geol. 166 (2000) 241–254.
[64] B.S. Kamber, A. Ewart, K.D. Collerson, M.C. Bruce, G.D. McDonald, Fluid-mobile trace element constraints on the role of slab melting and implications for Archaean crustal growth models, Contrib. Mineral. Petrol. 144 (2002) 38–56.
[65] M.B. Baker, P.J. Wyllie, High-pressure apatite solubility in carbonate-rich liquids: implications for mantle metasomatism, Geochim. Cosmochim. Acta 56 (1992) 3409–3422.
[66] R.L. Rudnick, W.F. McDonough, B.W. Chappell, Carbonatite metasomatism in the northern Tanzanian mantle: petrographic and geochemical characteristics, Earth Planet. Sci. Lett. 114 (1993) 463–475.
[67] C. Dupuy, J.M. Liotardand, J. Dostal, Zr/Hf fractionation in intraplate basaltic rocks: carbonate metasomatism in the mantle source, Geochim. Cosmochim. Acta 56 (1992) 2417–2423.
[68] K. Hoernle, G. Tilton, M.J. Le Bas, S. Duggen, D. Garbe-Schonberg, Geochemistry of oceanic carbonatites compared with continental carbonatites: mantle recycling of oceanic crustal carbonate, Contrib. Mineral. Petrol. 142 (2002) 520–542.
[69] G. Brey, W.R. Brice, D.J. Ellis, D.H. Green, K.L. Harris, I.D. Ryabchikov, Pyroxene–carbonate reactions in the upper mantle, Earth Planet. Sci. Lett. 62 (1983) 63–74.
[70] S. Foley, Vein-plus-wall-rock melting mechanisms in the lithosphere and the origin of potassic alkaline magmas, Lithos 28 (1992) 435–453.

[71] R.P. Rapp, N. Shimizu, M.D. Norman, G.S. Applegate, Reaction between slab-derived melts and peridotite in the mantle wedge: experimental constraints at 3.8 GPa, Chem. Geol. 160 (1999) 335–356.
[72] A. Yin, T.M. Harrison, Geologic evolution of the Himalayan–Tibetan orogen, Annu. Rev. Earth Planet Sci. 28 (2000) 211–280.
[73] Z.Q. Hou, H.W. Ma, K. Zaw, Y.Q. Zhang, M.J. Wang, Z. Wang, G.T. Pan, R.L. Tang, The Himalayan Yulong porphyry copper belt: produced by large-scale strike-slip faulting at Eastern Tibet, Econ. Geol. 98 (2003) 125–145.
[74] D. Fei, Regional structure in the northern part of the South China Sea and transition from continental crust to oceanic crust, J. Geophys. 26 (1983) 459–467.
[75] J.P. Liegeois, L. Latouche, M. Boughrara, J. Navez, M. Guiraud, The LATEA metacraton (Central Hoggar, Tuareg shield, Algeria): behaviour of an old passive margin during the Pan-African orogeny, J. Afr. Earth Sci. 37 (2003) 161–190.
[76] Y.G. Xu, M.A. Menzies, M.F. Thirlwall, G.H. Xie, Exotic lithosphere mantle beneath the western Yangtze craton: petrogenetic links to Tibet using highly magnesian ultrapotassic rocks, Geology 29 (2001) 863–866.
[77] O.F. Tuttle, N.L. Bowen, Origin of granite in the light of experimental studies in the system $NaAlSi_3O_8$–$KAlSi_3O_8$–SiO_2–H_2O, Geol. Soc. Am., Mem. 74 (1958) 153.
[78] A.J.R. White, B.W. Chappell, Granitoid types and their distribution in the Lachlan Fold Belt, southeastern Australia, Geol. Soc. Am., Mem. 159 (1983) 21–34.
[79] J.C. Duchesne, I.T. Berza, J.P. Liégeois, J. vander Auwera, Shoshonitic liquid line of descent from diorite to granite: the late Precambrian post-collisional Tismana pluton (South Carpathians, Romania), Lithos 45 (1998) 281–303.
[80] D.J. DePaolo, Trace element and isotopic effects of combined wallrock assimilation and fractional crystallization, Earth Planet. Sci. Lett. 53 (1981) 189–202.
[81] A. Ewart, J.J. Stipp, Petrogenesis of volcanic rocks of the central North Island, New Zealand, as indicated by a study of $^{87}Sr/^{86}Sr$ ratios, and Sr, Rb, K, U, and Th abundances, Geochim. Cosmochim. Acta 32 (1968) 699–736.
[82] R. Oyarzun, A. Marquez, J. Lillo, I. Lopez, S. Rivera, Giant versus small porphyry copper deposits of Cenozoic age in northern Chile: adakitic versus normal calc-alkaline magmatism, Miner. Depos. 36 (2001) 794–798.
[83] J.F. Xu, R. Shinjo, M.J. Defant, Q.A. Wang, R.P. Rapp, Origin of Mesozoic adakitic intrusive rocks in the Ningzhen area of east China: partial melting of delaminated lower continental crust?, Geology 30 (2002) 1111–1114.
[84] R.P. Castillo, P.E. Janney, R.S. Solidum, Petrology and geochemistry of Camiguia Island, Southern Phillippines: insight to the source of adakites and other lavas in a complex arc setting, Contrib. Mineral. Petrol. 134 (1999) 33–51.
[85] Y.Q. Zhang, Y.W. Xie, Chronology and Nd, Sr isotopic characteristics of the Ailaoshan-Jinshajiang alkali-rich intrusive rocks, Sci. China, Ser. D: Earth Sci. 27 (1997) 289–293.
[86] N. Morimoto, Nomenclature of pyroxenes, Fortschr. Mineral. 66 (1988) 237–252.
[87] M.J. Le Bas, R.W. Le Maitre, A. Streckeisen, B.A. Zanettin, A chemical classification of volcanic rocks based on the total alkaline-silica diagram, J. Petrol. 27 (1986) 745–750.
[88] W.V. Boynton, Cosmochemistry of the rare earth elements: meteorite studies, in: P. Henderson (Ed.), Rare Earth Element Geochemistry, Elsevier, Amsterdam, 1984, pp. 63–114.
[89] W.F. McDonough, S.S. Sun, Isotopic and geochemical systematics in Tertiary–recent basalts from southeastern Australia and implication for the sub-continental lithosphere, Geochim. Cosmochim. Acta 49 (1985) 2051–2067.
[90] K.H. Schmidt, P. Bottazzi, R. Vannucci, K. Mengel, Trace element partitioning between phlogopite, clinopyroxene and leucite lamproite melt, Earth Planet. Sci. Lett. 168 (1999) 287–299.
[91] Q. Zheng, Calculation of the Fe^{3+} and Fe^{2+} contents in silicate and Ti–Fe oxide minerals from epma data, Acta Mineral. Sin. 3 (1983) 55–62 (in Chinese with English abstract).